

Cogging Torque Reduction in Axial Flux PMSM with Different Permanent Magnet Combination

WANG Xiaoguang¹, LIU Cheng¹, ZHOU Sheng¹, WAN Ziwei¹, LIU Yi^{2*}

1. Hubei Key Laboratory for High-Efficiency Utilization of Solar Energy and Operation Control of Energy Storage System, School of Electrical and Electronic Engineering, Hubei University of Technology, Wuhan 430068, P.R.China;

2. School of Electrical and Electronic Engineering, Huazhong University of Science and Technology, Wuhan 430074, P.R.China

(Received 10 August 2021; revised 10 September 2021; accepted 25 September 2021)

Abstract: With the increasing requirement for the mechanical vibration and acoustic noise of the permanent magnet synchronous motor (PMSM) drive system, the demand for cogging torque reduction of PMSM has been considerably increased. To solve the problem of oversized cogging torque of axial flux PMSM, a rotor topology with hybrid permanent magnet is proposed to weaken the cogging torque. Firstly, the expression of the cogging torque of the axial flux motor is derived, and the influence of the pole-arc ratio of the permanent magnet on the cogging torque is analyzed. Secondly, the rotor structure with hybrid permanent magnet is adopted to reduce the cogging torque. According to the analytical analysis, the constraints of the size and pole-arc ratio between the hybrid permanent magnets are obtained, and the two permanent magnets related to the minimum cogging torque are determined. And the analysis results are verified by the finite element simulation. Furthermore, the motor performance with and without the hybrid permanent magnet is compared with each other. Finally, the cogging torque is significantly reduced by adopting a rotor structure with hybrid permanent magnets.

Key words: axial flux permanent magnet synchronous motor (AFPMSM); rotor structure; cogging torque; hybrid permanent magnet; pole-arc ratio

CLC number: TM341

Document code: A

Article ID: 1005-1120(2021)05-0726-11

0 Introduction

The axial flux permanent magnet synchronous motor (AFPMSM) has many advantages, such as high power density and short axial length, which is widely used in the application of electric vehicles^[1-3]. However, the deteriorate performance of noise, vibration, harshness (NVH) and poor reliability are appeared by the existence of cogging torque of the motor^[4].

In recent years, scholars have made many relevant researches on weakening methods for cogging torque of machine. Several methods are introduced to reduce the cogging torque of variable flux reluctance machines including asymmetrical rotor teeth,

circumferential rotor teeth pairing and rotor dummy slots^[5]. To reduce the cogging torque for hybrid axial field flux-switching permanent magnet machine, three cogging torque reduction methods by tangential displacement of stators, asymmetric rotor pole shape, and segment-twisted rotor are investigated^[6]. Cogging torque optimization of a flux memory pole-changing permanent magnet machine is presented by the Taguchi method, the response surface methodology, and the genetic algorithm^[7]. The analytical approach used to study cogging torque in axial flux permanent magnet (AFPM) machines can be as efficient as the 3-D finite element analysis (FEA) while saving a huge amount of time and necessitating less initial expertise^[8]. The analytical expression of cog-

*Corresponding author, E-mail address: liuyi82@hust.edu.cn.

How to cite this article: WANG Xiaoguang, LIU Cheng, ZHOU Sheng, et al. Cogging torque reduction in axial flux PMSM with different permanent magnet combination[J]. Transactions of Nanjing University of Aeronautics and Astronautics, 2021, 38(5):726-736.

<http://dx.doi.org/10.16356/j.1005-1120.2021.05.002>

ging torque of flux reversal permanent magnet motor is derived. The expression considers the small gap between two adjacent magnets belonging to the same sub tooth. Furthermore, the optimal dimensions of the space gap are obtained analytically for cogging torque minimization^[9]. The relation between the permanent magnet (PM) and the harmonic order of the cogging has been studied by the analytical method, and the pole-slot coordination with minimum cogging torque has been derived^[10]. An improved semi-analytical model is proposed to investigate the cogging torque of AFPM under angular misalignment, and it is more accurate for angular misalignment^[11]. The influence of magnet pole-arc ratio on cogging torque of PM motor was studied in Refs. [12-13], and the cogging torque is effectively weakened by optimizing the pole-arc ratio.

The optimized shape of PM can weaken the cogging torque of PMSM. An asymmetrical V-type rotor configuration is adopted to reduce cogging torque and torque ripple^[14]. The application position of skew in order to reduce the cogging torque of a magnetic geared synchronous motor (MGM) is studied^[15]. PM is shifted by a certain angle along the radial direction, which reduces the cogging torque and torque ripple^[16-17]. However, the manufacturing process of PM is complicated. Dividing the PM into two pieces and only shifting one of them by a certain angle can also effectively suppress the cogging torque without increasing the difficulty of the manufacturing process of PM^[18].

In addition, many scholars use the method of combining magnetic poles to weaken cogging torque of surface-mount radial flux motors. A novel combined rectangle-shaped magnet arrangement was proposed and investigated for cogging torque minimization in Ref. [19]. In Ref. [20], two materials, NdFeB and samarium cobalt, were mixed along the axial direction, and the best combination of pole-arc ratio was obtained through analytical calculation^[20]. In Ref. [21], two PMs were combined to weaken the harmonics of air-gap magnetic field, and the optimal combination of magnet pole-arc ratio was obtained by zooming optimization algorithm. This paper also mentioned PMs with different thicknesses. The cogging torque is reduced by optimizing the air

gap magnetic field. Based on the results of literature survey, the reduction of cogging torque of radial flux permanent magnet motor has been deeply studied^[22]. Other scholars have studied the surface mounted radial permanent magnet hybrid motor. Through calculation and simulation analysis, the hybrid permanent magnet motor can not only reduce the permanent magnet cost of the motor, but also weaken the cogging torque of the motor, thus reducing the torque ripple^[23]. The above methods proposed by scholars can effectively reduce the cogging torque of the motor. However, these methods either have difficulties in machining and motor assembly, or some methods will weaken the air gap flux density of the motor. Considering the weakening method of cogging torque of radial flux permanent magnet motor, the reduction of cogging torque of axial flux motor is analyzed according to the characteristics of axial flux permanent magnet motor.

In order to weaken the cogging torque without increasing the processing technology and cost, a rotor structure with hybrid permanent magnets is proposed. In this paper, a 7.5 kW yokeless and segmented armature (YASA) axial flux permanent magnet motor is taken as the research object, and the structure and basic parameters of the motor are shown in Fig.1 and Table 1. First, an energy method is used to calculate the cogging torque of AF-PMSM. The cogging torque is affected by the magnet pole-arc ratio. Then, the cogging torque with different pole-arc ratios are analyzed by the analytical method when PMs are mixed. The pole-arc ratio is obtained by the graphic method when cogging torque is minimum. Finally, the finite element simulation is used to verify the accuracy of the constraints.

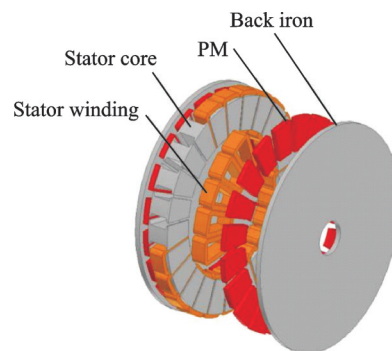


Fig.1 Topology structure of the YASA motor

Table 1 Basic parameters of the YASA motor

Parameter	Value
Rated power / kW	7.5
Peak power / kW	15
Rated torque / (N·m)	51.5
Peak torque / (N·m)	103
Rated speed / (r·min ⁻¹)	1 390
Peak speed / (r·min ⁻¹)	5 500
DC bus voltage / V	158
Number of poles	20
Number of slots	24
Motor outer diameter / mm	200
Motor inner diameter / mm	120
Axial length / mm	24

1 Analysis of Cogging Torque of Axial Flux Motor

1.1 Calculation of cogging torque

The following assumptions are made for the analytical calculation of cogging torque: (1) The permeability of the core is infinite. (2) The permeability of PM is the same as air. (3) The air gap flux density is uniformly distributed in the radial direction.

Cogging torque is produced by the interaction between PM and iron core when AFPMSM is not powered, and it is the negative derivative of the magnetic field energy W relative to the position angle α , shown as

$$T_{\text{cog}} = -\frac{\partial W}{\partial \alpha} \quad (1)$$

The energy stored in the magnetic field can be approximately regarded as the energy in PM and air gap, so it can be expressed as

$$W \approx W_{\text{airgap+PM}} = \frac{1}{2\mu_0} \int_V B_r^2(\theta) \left(\frac{h_m(\theta)}{h_m(\theta) + \delta(\theta, \alpha)} \right)^2 dV \quad (2)$$

where μ_0 is the permeability of air, α the angle between the center line of a specified PM and tooth, B_r the remanence density of PM, h_m the length of the magnetization direction of PM, δ the effective air gap length, θ the angle of change in the direction of rotation of the motor and V the air gap volume, as shown in Fig.2.

If PMs are evenly distributed, the Fourier ex-

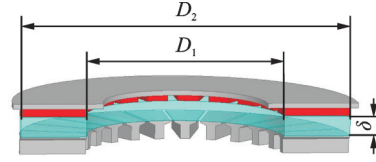


Fig.2 Axial motor model

pansion of B_r^2 can be expressed as

$$B_r^2(\theta) = \alpha_p B_r^2 + \sum_{n=1}^{\infty} B_m \cos(2np\theta) \quad (3)$$

where α_p is the pole-arc ratio of PM and p the number of rotor poles.

The Fourier expansion of $[h_m(\theta)/h_m(\theta) + \delta(\theta, \alpha)]^2$ can be expressed as

$$\left(\frac{h_m(\theta)}{h_m(\theta) + \delta(\theta, \alpha)} \right)^2 = \left(\frac{h_m}{h_m + \delta} \right)^2 + \sum_{n=1}^{\infty} G_n \cos[nZ(\theta + \alpha)] \quad (4)$$

where G_n is the Fourier expansion coefficient of the relative permeability function of motor air gap and Z the number of motor stator slots.

The volume of the air gap V is

$$V = \frac{\pi(D_2^2 - D_1^2)\delta}{2} \quad (5)$$

where D_1 and D_2 are the machine diameters at inner and outer surfaces, respectively.

Substituting the above analysis results into Eq.(1), the cogging torque of AFPMSM can be expressed as

$$T_{\text{cog(A)}} = \frac{\pi\delta}{4\mu_0} (D_2^2 - D_1^2) \sum_{n=1}^{\infty} nN_L G_n B_m \sin(nN_L \alpha) \quad (6)$$

where N_L is the least common multiple of the number of motor stator slots and the number of rotor poles.

1.2 Influence of pole-arc ratio on cogging torque

Eq.(6) indicates that B_m has a greater influence on the cogging torque, which can be expressed as

$$B_m = \frac{2}{n\pi} B_r^2 \sin(n\alpha_p \pi) \quad (7)$$

where n is an integer. It can make $nZ/2p$ as an integer. Furthermore, there are infinite integers n that satisfy above condition. In addition, n is defined to be arranged from small to large as $n_1, n_2, n_3, \dots, n_n$. p is the number of pole pairs, and α_p is the pole-arc ratio of PM. The number of cycles of cogging torque can be determined (that is, n_1 can be deter-

mined) when the number of poles and slots are determined. The axial flux permanent magnet motor studied in this paper is 24 slot/20 pole. According to the above analysis, the period of cogging torque is 5, i.e., $n_1=5$, and the obtained $nZ/2p(3, 6, 9, \dots)$ times harmonic of the air gap flux density has an influence on cogging torque. According to the graphical method, substituting $n=5, 10, 15$ and 20 into Eq.(7), the curve of B_m changing with pole-arc ratio α_p , is shown in Fig.3.

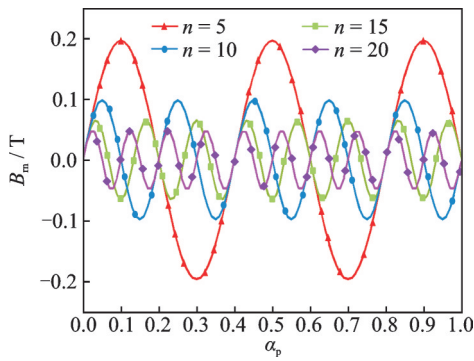


Fig.3 Graphical analysis of B_m and α_p

Combining Eqs. (6, 7), the expression of the cogging torque of AFPMSM can be obtained as

$$T_{\text{cog}(A)} = \frac{\delta}{2\mu_0} (D_2^2 - D_1^2) \sum_{n=1}^{\infty} N_L G_n B_r^2 \sin(n\alpha_p\pi) \sin(nN_L\alpha) \quad (8)$$

It can be obtained from Fig.3 and Eq.(8) that, as α_p changes in the range of $[0, 1]$, B_m also changes periodically, and $T_{\text{cog}(A)}$ is proportional to B_m , so $T_{\text{cog}(A)}$ will also change periodically with α_p .

2 Hybrid Permanent Magnet Method

2.1 Analytical analysis

In this paper, a rotor topology with hybrid permanent magnet is adopted to reduce the cogging torque. The structure of the motor with hybrid permanent magnet is shown in Fig.4. This machine uses two kinds of PMs with different materials to excite the motor, and the two PMs are arranged radially, as shown in Fig.5.

When two different PMs are mixed in the radial direction, it can be considered that the magnetic

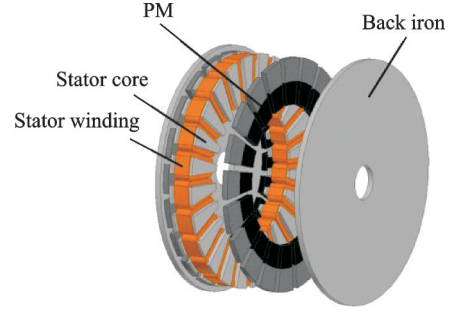


Fig.4 Structure of hybrid permanent magnet

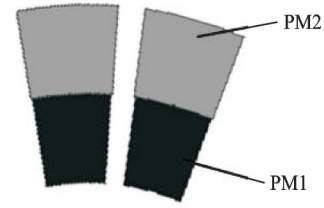


Fig.5 Arrangement of hybrid permanent magnets

circuits generated by the two PMs are in parallel, and the motor with hybrid permanent magnet can be equivalent to two axial flux motors using PM1 and PM2, respectively. The cogging torque of the motor with hybrid permanent magnet can be equivalent to the superposition of two axial flux motors^[20]. Let the cogging torque of two axial flux motors be $T_{\text{cog}(A1)}$ and $T_{\text{cog}(A2)}$, shown as

$$\left\{ \begin{array}{l} T_{\text{cog}(A1)} = \frac{\delta}{2\mu_0} B_{r1}^2 (D_{12}^2 - D_{11}^2) \cdot \\ \quad \sum_{n=1}^{\infty} N_L G_{n1} \sin(n\alpha_{p1}\pi) \sin(nN_L\alpha) \\ T_{\text{cog}(A2)} = \frac{\delta}{2\mu_0} B_{r2}^2 (D_{22}^2 - D_{21}^2) \cdot \\ \quad \sum_{n=1}^{\infty} N_L G_{n2} \sin(n\alpha_{p2}\pi) \sin(nN_L\alpha) \end{array} \right. \quad (9)$$

where D_{12} and D_{11} are the outer diameter and inner diameter of the motor with PM1, D_{22} and D_{21} the outer diameter and inner diameter of the motor with PM2, B_{r1} and B_{r2} the remanences of PM1 and PM2, and α_{p1} and α_{p2} the pole-arc ratios of PM1 and PM2. When the motor with hybrid permanent magnet is in a steady state, the air gap flux density is uniform. Therefore, the air gap flux amplitude of two motors is equal, and it can be obtained as

$$G_n = G_{n1} = G_{n2} \quad (10)$$

Assuming that the PM has the same remanence, the cogging torque of two axial flux motors is to be superimposed on each other according to

Eq.(10), which can be expressed as

$$\begin{aligned} B_{r1}^2 (D_{12}^2 - D_{11}^2) = \\ B_{r2}^2 (D_{22}^2 - D_{21}^2) = B_r^2 (D_o^2 - D_i^2) \end{aligned} \quad (11)$$

where B_r is the equivalent remanence of the motor with hybrid permanent magnet, and D_o and D_i are the machine diameters at outer and inner surfaces. The cogging torque of this machine can be expressed as

$$\begin{aligned} T_{\text{cog}(\Lambda)} = \frac{\pi \delta}{4\mu_0} (D_o^2 - D_i^2) \cdot \\ \sum_{n=1}^{\infty} n N_L G_n B_{m(h)} \sin(n N_L \alpha) \end{aligned} \quad (12)$$

where $B_{m(h)}$ is the superposition of B_m of two motors, which can be expressed as

$$\begin{aligned} B_{m(h)} = B_{m1} + B_{m2} = \\ \frac{2}{n\pi} B_{r1}^2 \sin(n\alpha_{p1}\pi) + \frac{2}{n\pi} B_{r2}^2 \sin(n\alpha_{p2}\pi) \end{aligned} \quad (13)$$

When the operating point of the PM in the motor with hybrid permanent magnet is unchanged, the air gap flux density and pole-arc ratio of the two PMs should meet

$$B_{\delta 1} \alpha_{p1} = B_{\delta 2} \alpha_{p2} \quad (14)$$

The air gap flux density of surface mount motor is proportional to the remanence of PM. Therefore, the relationship between the pole-arc ratio and remanence of two PMs can be summarized as

$$B_{r1} \alpha_{p1} = B_{r2} \alpha_{p2} \quad (15)$$

Combining Eqs. (10—12), the expression of $B_{m(h)}$ can be obtained as

$$B_{m(h)} = \frac{2}{n\pi} \left[B_{r1}^2 \sin(n\alpha_{p1}\pi) + B_{r2}^2 \sin\left(n \frac{B_{r1}}{B_{r2}} \alpha_{p1}\pi\right) \right] \quad (16)$$

Eq.(16) takes α_{p1} as the only variable. Substituting Eq.(11, 16) into Eq.(12), the cogging torque of the motor with hybrid permanent magnet is

$$\begin{aligned} T_{\text{cog}(\Lambda)} = \frac{\delta}{2\mu_0} B_r^2 (D_o^2 - D_i^2) \sum_{n=1}^{\infty} N_L G_n \cdot \\ \left[\sin(n\alpha_{p1}\pi) + \sin\left(n \frac{B_{r1}}{B_{r2}} \alpha_{p1}\pi\right) \right] \sin(n N_L \alpha) \end{aligned} \quad (17)$$

It can be obtained by Eq.(17) that $T_{\text{cog}(\Lambda)}$ is the sine function of α_{p1} . The sine function in Eq.(17) is represented by k , shown as

$$k = k_1 + k_2 = \sin(n\alpha_{p1}\pi) + \sin\left(n \frac{B_{r1}}{B_{r2}} \alpha_{p1}\pi\right) \quad (18)$$

$T_{\text{cog}(\Lambda)}$ takes the minimum value when α_{p1}

makes k zero. According to Eq.(18) and the remainences of two kinds of PMs, the curve of k changing with α_{p1} can be obtained by the graphical method. In this paper, N38UH and N35UH are selected for mixing, the remanences of them are 1.25 T and 1.2 T, respectively. Put the remanence into Eq.(18), the curve of the value of k changing with α_{p1} under different harmonic orders can be obtained through the graphical method. The results are shown in Fig.6.

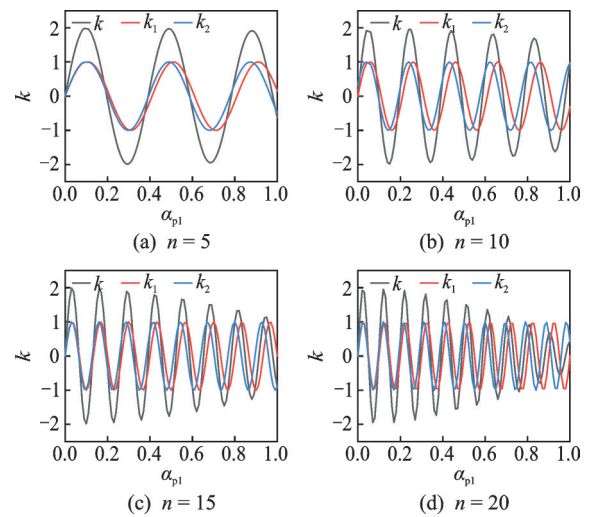


Fig.6 Analysis results of k of hybrid permanent magnet motor under different harmonic orders

According to Fig.6, when $B_{m1} > 0$ and $B_{m2} < 0$, or $B_{m1} < 0$ and $B_{m2} > 0$, B_m corresponding to the two PMs in the motor with hybrid permanent magnet weaken each other, and the cogging torque is reduced. The minimum of $T_{\text{cog}(\Lambda)}$ can be got when $B_{m1} = -B_{m2}$ and B_m is zero. With the increase of n and α_p , the amplitude of k shows a tendency of decreasing, which indicates that the rotor topology with hybrid permanent magnet has a very obvious effect on weakening the cogging torque generated by higher harmonics. It can be obtained by analysis that k is to be zero when $\alpha_{p1} = 0.2, 0.39, 0.5, 0.78$ and 0.97 , meanwhile, $T_{\text{cog}(\Lambda)}$ is minimum.

2.2 Finite-element verification

The finite element simulation method is used to verify the correctness of theoretical analysis. Two motors studied in this paper are axial flux motors, i.e., NdFeB motor with one kind of NdFeB and a hybrid permanent magnet motor with a mixture of

two NdFeBs. For NdFeB motor, the inner diameter and outer diameter of PM are equal to the inner diameter and outer diameter of motor. The size of the PM of hybrid permanent magnet motor needs to be calculated through the constraint conditions in Eq.(11) and the inner and outer diameters of the motor are

$$\begin{cases} B_{m1}^2 (D_{12}^2 - D_{11}^2) = B_{m1}^2 (D_{22}^2 - D_{21}^2) \\ D_{12}^2 = D_{21}^2 \\ D_{11}^2 = 120 \\ D_{22}^2 = 200 \end{cases} \quad (19)$$

The calculation results show that $D_{12} = D_{21} = 163$ mm. The materials and dimensions of the PMs of the two motors are shown in Table 2.

Table 2 PM sizes of two motors

Material	Part	Diameter/mm	
		NdFeB motor	Hybrid PM motor
N38UH	Outer	200	163
	Inner	120	120
N35UH	Outer		200
	Inner		163

The cogging torque of NdFeB motor with different magnet pole-arc ratio is simulated by FEM and the results are shown in Fig.7.

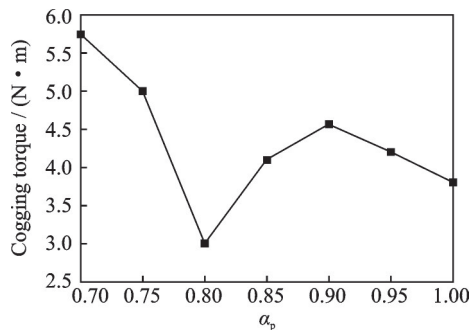


Fig.7 Simulation results of cogging torque of NdFeB motor under different α_p

Fig.7 shows that the cogging torque of NdFeB motor reaches the maximum of 5.7 N·m in the simulation range when α_p is 0.7, and reaches the minimum of 3 N·m when α_p is 0.8. It can be seen from Figs. 2, 6 that the cogging torques with different magnet pole-arc ratios obtained by the analytical method and the finite element simulation have the same trends, indicating that the graphical method in Fig.6 has a certain accuracy.

Fig.6 shows that the theoretical pole-arc ratio of N38UH is obtained when the cogging torque of hybrid permanent magnet motor is the smallest. The pole-arc ratio of N35UH is obtained by Eq.(15), and the results are shown in Table 3.

Table 3 Simulation results of polar-arc ratio combination

Combination	α_{p1}	α_{p2}	Cogging torque / (N·m)
1	0.20	0.21	1.74
2	0.39	0.4	2.06
3	0.59	0.61	2.21
4	0.78	0.81	1.63

According to Table 3, when the pole-arc ratios of N38UH and N35UH are 0.78 and 0.81, respectively, the cogging torque is the smallest. And the greater the pole-arc ratio, the stronger the torque output capacity, which is beneficial to improving torque density of the motor. Therefore, this paper chooses the pole-arc ratios of the two PMs to be 0.78 and 0.81.

Constraints of magnet pole-arc ratio are determined by Eq.(15). According to the results obtained above, the cogging torque of hybrid permanent magnet motor can obtain the minimum when α_{p1} and α_{p2} are 0.78 and 0.81, respectively. To verify this conclusion, keep α_{p1} unchanged, let α_{p2} be mixed in the range of [0.75, 0.85], and the cogging torque of each group of hybrid permanent magnet structure is analyzed by the finite element method.

The simulation results of permanent magnet pole-arc ratio constraints are shown in Fig.8. As shown in Fig.8, the FEA results of constraint conditions of magnet pole-arc ratio are consistent with the analytical results, and the accuracy of constraint conditions in Eq.(15) is verified.

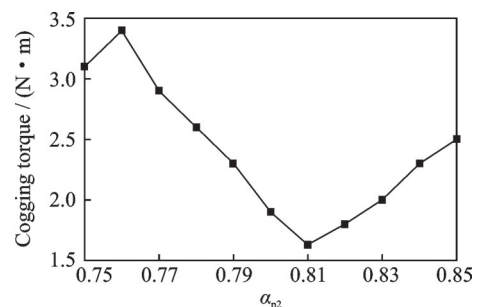


Fig.8 Simulation results of pole-arc ratio constraints of PMs

Since the inner and outer diameters and the positions of two kinds of PMs of the motor have been determined, the inner diameter of PM1 $D_{11}=120$ mm and the outer diameter of PM2 $D_{22}=200$ mm. Meanwhile, there is no gap in the radial direction of the two PMs. Therefore, the outer diameter of PM1 D_{12} and the inner diameter of PM2 D_{21} are equal. In order to verify the accuracy of constraint conditions, D_{12} is used as a variable to simulate the cogging torque of hybrid permanent magnet motor when D_{12} changes within the range of $[158, 167]$. The results are shown in Fig.9.

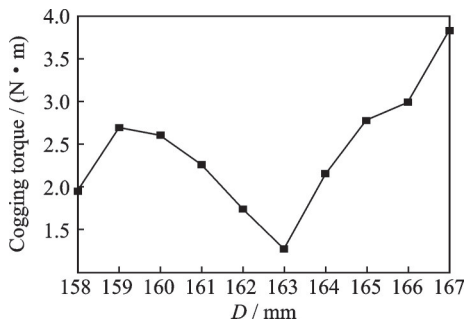


Fig.9 Simulation results of permanent magnet pole-arc ratio constraints

It can be seen from Fig.9 that the simulation result of constraint condition of the permanent magnet size is consistent with the analytical results, which verifies the accuracy of constraint condition in Eq.(11).

Fig.6 indicates that the cogging torque of hybrid PM motor is the smallest when $\alpha_{p1}=0.78$. To verify the conclusions drawn in Fig.6, make α_{p1} change within the range of $[0.7, 0.84]$, calculate α_{p2} by Eq.(15), and perform finite element simulation analysis on the combination of pole-arc ratio of different PM. The results are shown in Fig.10.

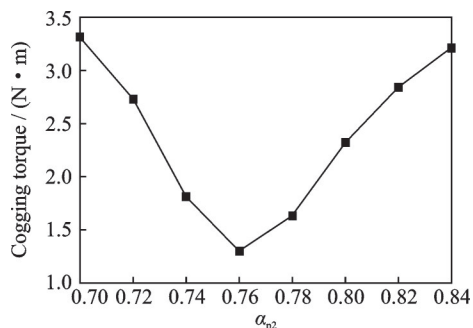


Fig.10 Simulation results of α_{p1} and motor cogging torque

It can be seen from Fig.10 that with the increase of PM1 pole-arc ratio, the cogging torque first decreases and then increases. The cogging torque is minimum when $\alpha_{p1}=0.76$ and $\alpha_{p2}=0.79$. The analytical calculation results show that the cogging torque is the smallest when $\alpha_{p1}=0.78$ and $\alpha_{p2}=0.81$, there is a 2.6% error between the simulation and calculation results. It is because that the graphical method is based on the derivation of the cogging torque of AFPMSM. Several assumptions are used in the derivation process of cogging torque, for example, the magnetic permeability of the motor is infinite, the internal magnetic flux of the motor will not saturate, and the motor is also assumed to be slotless when calculating B_m , so a certain error is generated in the calculation result.

Summarizing the above analysis, the size and pole-arc ratio of two kinds of PMs in hybrid permanent magnet motor are shown in Table 4.

Table 4 Parameters of two kinds of PMs in hybrid permanent magnet motor

Parameter	N38UH	N35UH
Outer diameter / mm	163	200
Inner diameter / mm	120	163
Pole-arc ratio	0.76	0.79

3 Analysis and Comparison of Performance

The performance of NdFeB motor and hybrid permanent magnet motor are compared. The structures of the two motors are shown in Fig.1 and Fig.4, respectively. Due to the pole-arc ratio of N38UH in hybrid permanent magnet motor is 0.76, for ease of comparison, the NdFeB motor uses permanent magnets of the same material and pole-arc ratio.

Fig.11 shows the spatial distribution of the radial air gap magnetic flux density over one pole of the proposed motor. It can be seen that the air gap magnetic flux density amplitude is not the same in the x -axis direction. The magnetic flux density amplitude is larger in the range from $x=60$ mm to $x=81.5$ mm. This part of the magnetic flux density is produced by PM1, and the remaining part of the air

gap magnetic flux density is produced by PM2. The interaction of different air gap flux densities in the radial direction can reduce cogging torque.

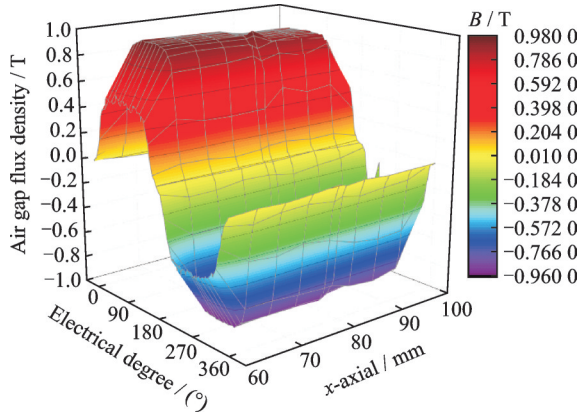


Fig.11 Space distribution of radial air gap flux density over one pole

The magnetic flux density distribution on the rotor with hybrid permanent magnet is shown in Fig.12. It can be seen from Fig.12 that the magnetic flux density on the surface of PM1 is greater than that on the surface of PM2, which is also consistent with the above analysis.

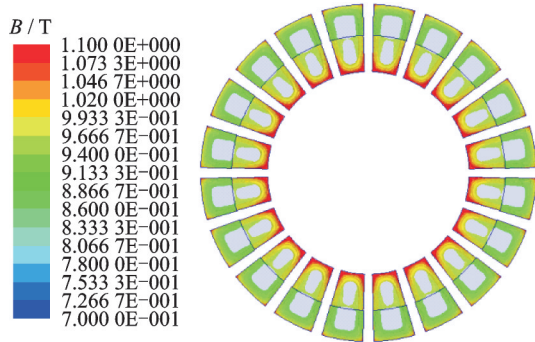


Fig.12 Magnetic flux density distribution on rotor with hybrid permanent magnet

The no-load back electromotive force (EMF) and the Fourier analysis waveform before and after hybrid permanent magnet are shown in Figs.13, 14. It can be seen from Figs.13, 14 that after hybrid permanent magnet the back EMF waveforms remain symmetrical, and the amplitude of the fundamental back EMF is only reduced from 78.8 V to 75 V, reduced by 4.5%, and the total harmonic distortion (THD) is increased from 2.7% to 3.7%. It is because that the application of the hybrid permanent magnet method brings double PMs, resulting in in-

creasing of magnetic flux leakage and decreasing of main magnetic flux. Therefore, the amplitude of the fundamental no-load back EMF decreases, and the back EMF has an effect on output torque. The greater the amplitude of back EMF fundamental wave, the greater the average torque output by the motor. The harmonic content of the back EMF will affect the pulsation of the output torque. The torque pulsation will increase with the increase of the harmonics.

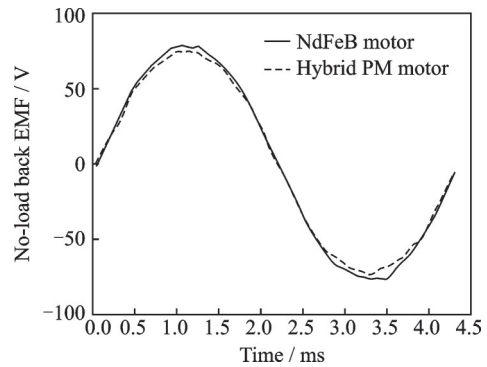


Fig.13 Waveforms of no-load back EMF of two motors

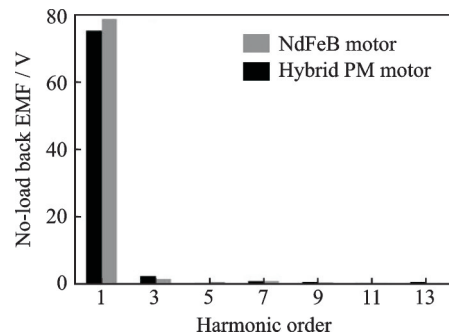


Fig.14 Fourier analysis of two motors with no-load back EMF

The cogging torque waveforms of the two motors are shown in Fig.15. It can be seen from Fig.15 that the cogging torque of the hybrid permanent magnet is reduced from 4.6 N·m to 1.3 N·m, a de-

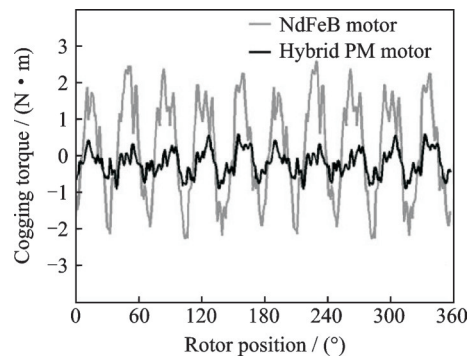


Fig.15 Cogging torque waveforms of two motors

crease of 71.7%. It indicates that the method of hybrid permanent magnet can effectively reduce the cogging torque.

The rated torque waveforms of the two motors at 39 A are shown in Fig. 16. It can be seen from Fig. 16 that the average torque of hybrid permanent magnet motor is reduced from 53.4 N·m to 51.9 N·m, and the torque ripple is decreased from 14.1% to 5.6%. Due to the increase of the magnetic flux leakage after the rotor topology with hybrid permanent magnet is adopted, the torque output capacity is reduced, and the cogging torque is also decreased, thus the torque ripple is reduced.

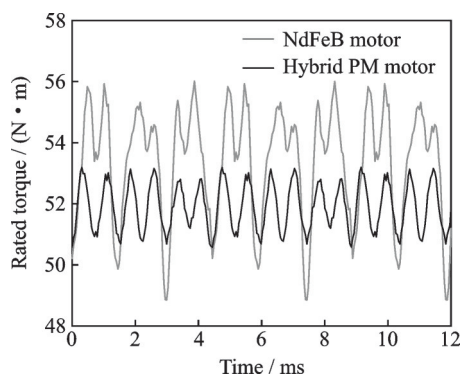


Fig. 16 Rated torque waveforms of two motors

Fig. 17 shows the torque ripple curves changing with current I . As shown in Fig. 17, the torque ripple of the two motors shows a downward trend with the increase of I . And the proposed hybrid permanent magnet motor has the lower torque ripple than the NdFeB motor at each current. When $I=4$ A, the ripple value of the hybrid permanent magnet motor is 34.2%, which is 57.5% less than that of the NdFeB one. When $I=40$ A, the proposed hybrid permanent magnet motor is 6.37%, which is 43.37% less than that of the NdFeB one. This rotor topology is also proved to be effective to reduce the torque ripple, which is consistent with the analysis results in Figs. 13, 14.

The peak torque waveforms of two motors are shown in Fig. 18. It can be seen from Fig. 18 that after the rotor structure with hybrid permanent magnet is adopted, the peak torque is reduced from 103.3 N·m to 101.7 N·m, and the torque ripple is decreased from 9.5% to 4.8%.

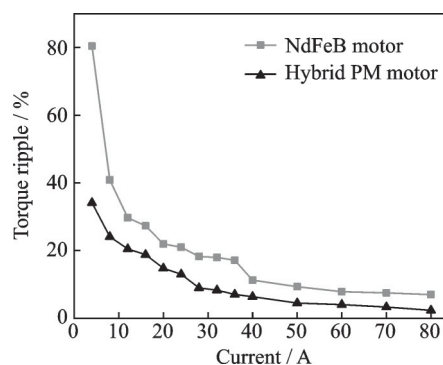


Fig. 17 Torque ripple versus current

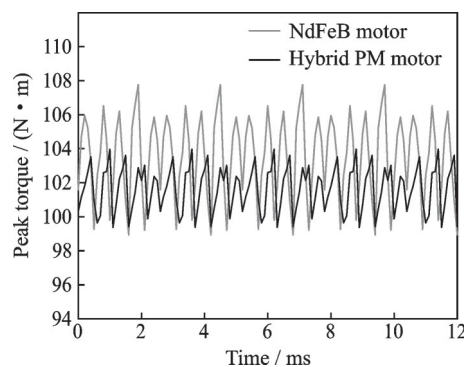


Fig. 18 Peak torque waveforms of two motors

The cogging torque, average torque, torque ripple and efficiency of two motors are compared in Table 5. For ease of comparison, set the two motors to the same volume. It can be seen from Table 5 that when the rotor structure with hybrid permanent magnet is adopted, the cogging torque drops from 4.6 N·m to 1.3 N·m, a decrease of 71.7%. The torque drops from 53.4 N·m to 51.9 N·m, reduced by 2.8%, and the torque ripple drops from 14.1% to 5.7%, reduced by 59.6% in rated condition. In peak condition, the torque drops from 103.3 N·m

Table 5 Performance comparison of two motors

Project		NdFeB motor	Hybrid PM motor
Cogging torque / (N·m)		4.6	1.3
Rated condition	Rated torque/(N·m)	53.4	51.9
	Torque ripple/%	14.1	5.7
	Peak torque/(N·m)	103.3	101.7
Peak condition	Torque ripple/%	9.5	4.8
	Volume/cm ³	1 570	1 570
Permanent magnet mass/kg		1.153	1.178

to 101.7 N·m, which is reduced by 1.5%, and the torque ripple drops from 9.5% to 4.8%, which is reduced by 49.5%. And the amount of permanent magnets of the two motors is almost the same. Therefore, the method of hybrid permanent magnet can improve the torque performance of the motor.

4 Conclusions

In this paper, a rotor topology with hybrid permanent magnet of AFPMSM is presented and the cogging torque is reduced. The major contributions of this paper are:

(1) The cogging torque can be reduced when the size and pole-arc ratio of the two PMs strictly followed the constraints in this paper.

(2) There exists 2.6% error between the optimal pole-arc ratio obtained by the finite element simulation and analytical results due to the use of hypothetical theory in the analysis of cogging torque.

(3) By using the hybrid permanent magnet motor rotor topology, the magnetic leakage increases, which reduces the no-load back-EMF and the rated torque by 4.5% and 1.9%, respectively.

(4) The cogging torque and torque ripple reductions are 71.7% and 59.6%, respectively, by the topology of hybrid permanent magnet.

References

- [1] HUANG X, TAN Q, LI L, et al. Winding temperature field model considering void ratio and temperature rise of a permanent-magnet synchronous motor with high current density[J]. *IEEE Transactions on Industrial Electronics*, 2017, 64(3): 2168-2177.
- [2] AYDIN M, GULEC M. A new coreless axial flux interior permanent magnet synchronous motor with sinusoidal rotor segments[J]. *IEEE Transactions on Magnetics*, 2016, 52(7): 1-4.
- [3] PEI Y, WANG Q, BI Y, et al. A novel structure of axial flux permanent magnet synchronous machine with high torque density for electrical vehicle applications[C]//*Proceedings of IECON 2017—The 43rd Annual Conference of the IEEE Industrial Electronics Society*. Beijing, China: IEEE, 2017: 1717-1722.
- [4] GAO J, WANG G, LIU X, et al. Cogging torque reduction by elementary-cogging-unit shift for permanent magnet machines[J]. *IEEE Transactions on Magnetics*, 2017, 53(11): 1-5.
- [5] LIU Y, YIN J, GONG B, et al. Comparative analysis of cogging torque reduction methods of variable flux reluctance machines for electric vehicles[C]//*Proceedings of the 20th International Conference on Electrical Machines and Systems (ICEMS)*. Sydney, NSW:[s.n.], 2017:1-6.
- [6] XU D, LIN M, FU X, et al. Cogging torque reduction of a hybrid axial field flux-switching permanent-magnet machine with three methods[J]. *IEEE Transactions on Applied Superconductivity*, 2016, 26(4): 1-5.
- [7] WANG D, LIN H, YANG H, et al. Cogging torque optimization of flux memory pole-changing permanent magnet machine[J]. *IEEE Transactions on Applied Superconductivity*, 2016, 26(4): 1-5.
- [8] TIEGNA H, AMARA Y, BARAKAT G. Study of cogging torque in axial flux permanent magnet machines using an analytical model[J]. *IEEE Transactions on Magnetics*, 2014, 50(2): 845-848.
- [9] ZHU X, HUA W. An improved configuration for cogging torque reduction in flux-reversal permanent magnet machines[J]. *IEEE Transactions on Magnetics*, 2017, 53(6): 1-4.
- [10] PETKOVSKA L, CVETKOVSKI G, LEFLEY P. Analysis of the stator topology impact on cogging torque for surface permanent magnet motor[J]. *COMPEL—The International Journal for Computation and Mathematics in Electrical and Electronic Engineering*, 2015, 34(2):456-474.
- [11] GUO B, HUANG Y. Analytical modeling of angular misalignment for axial flux PM machines: Effects on cogging torque[C]//*Proceedings of 2018 IEEE International Magnetic Conference (INTERMAG)*. Singapore:[s.n.], 2018.
- [12] SHI J T, LIU X, WU D, et al. Influence of stator and rotor pole arcs on electromagnetic torque of variable flux reluctance machines[J]. *IEEE Transactions on Magnetics*, 2014, 50(11):1-4.
- [13] DU Z S, LIPO T A. Reducing torque ripple using axial pole shaping in interior permanent magnet machines[J]. *IEEE Transactions on Industry Applications*, 2019, 56(1):148-157.
- [14] WU R, QIANG X, LI Q, et al. Reduction of cogging torque and torque ripple in interior PM machines with asymmetrical V-type rotor design[J]. *IEEE Transactions on Magnetics*, 2016, 52(7):1-5.
- [15] JO I H, LEE H W, JEONG G, et al. A study on the reduction of cogging torque for the skew of a magnetic geared synchronous motor[J]. *IEEE Transactions on Magnetics*, 2019, 55(2):1-5.
- [16] XU L, XU Y, GONG J. Analysis and optimization of cogging torque in yokeless and segmented armature ax-

- ial-flux permanent-magnet machine with soft magnetic composite core[J]. IEEE Transactions on Magnetics, 2018, 54(11):1-5.
- [17] LIU G, DU X, ZHAO W, et al. Reduction of torque ripple in inset permanent magnet synchronous motor by magnets shifting[J]. IEEE Transactions on Magnetics, 2017, 53(2):1-13.
- [18] HUANG M S, CHEN P C, HUANG Y S, et al. Reduce the cogging torque of axial flux permanent magnet synchronous motor for light electric vehicle applications[C]//Proceedings of IEEE International Conference on Industrial Technology. Taipei, Taiwan, China: IEEE, 2016:193-197.
- [19] XIAO L, JIAN L, QU R, et al. Cogging torque analysis and minimization of axial flux PM machines with combined rectangle-shaped magnet[J]. IEEE Transactions on Industry Applications, 2017, 53(2):1018-1027.
- [20] HARISUDHA K, AFROSE S S, SURESH K. Different pole arc and different magnet combination to reduce the cogging torque in PMDC motors[C]// Proceedings of 2017 IEEE International Conference on Power, Control, Signals and Instrumentation Engineering (ICPCSI). Chennai, India: IEEE, 2017:2765-2769.
- [21] DOSIEK L, PILLAY P. Cogging torque reduction in permanent magnet machines[J]. IEEE Transactions on Industry Applications, 2007, 43(6):1565-1571.
- [22] WANG K, ZHU Z Q, OMBACH G. Torque enhancement of surface-mounted permanent magnet machine using third-order harmonic[J]. IEEE Transactions on Magnetics, 2014, 50(3):104-113.
- [23] BAO Xiaohua, WU Changjiang, FANG Jinlong. Method of reducing cogging torque of surface mounted permanent magnet synchronous motor by axial permanent magnet combination[J]. Transactions of China Electrotechnical Society, 2018, 33(18):4231-4238. (in Chinese)
- Acknowledgement** This work was supported by the Natural Science Foundation of Hubei Province (No.2019CFB759).
- Authors** Dr. WANG Xiaoguang received the Ph.D. degree in electrical engineering from Tianjin University, Tianjin, in 2015. He is currently a lecturer in the School of Electrical and Electronic Engineering, Hubei University of Technology. His research interests include electrical machines and motor drives.
- Dr. LIU Yi received the Ph.D. degree in high voltage and insulation technology from Huazhong University of Science and Technology (HUST) in 2013. He is currently an associate professor in School of Electrical and Electronic Engineering, HUST, with a focus on triggering characteristic and generator design of high-power spark gap switches.
- Author contributions** Dr. WANG Xiaoguang contributed to the background of the study and designed the study. Mr. LIU Cheng contributed to theoretical analysis of the model and prepared the manuscript. Mr. ZHOU Sheng and Mr. WAN Ziwei contributed to finite element modeling and the data for analysis. Dr. LIU Yi revised and modified the manuscript. All authors commented on the manuscript draft and approved the submission.
- Competing interests** The authors declare no competing interests.

(Production Editor: SUN Jing)

轴向磁通混合永磁电机齿槽转矩削弱方法研究

王晓光¹, 刘 城¹, 周 晟¹, 万子威¹, 刘 毅²

(1. 湖北工业大学电气与电子工程学院, 太阳能高效利用及储能运行控制湖北省重点实验室, 武汉 430068, 中国; 2. 华中科技大学电气与电子工程学院, 武汉 430074, 中国)

摘要: 随着对永磁同步电机(Permanent magnet synchronous motor, PMSM)驱动系统机械振动和噪声的要求不断提高,对降低永磁同步电机齿槽转矩的需求也大大增加。为了解决轴向PMSM齿槽转矩过大的问题,提出了一种带有混合永磁体的转子拓扑结构来削弱齿槽转矩。首先,推导了轴向磁通电机齿槽转矩的表达式,分析了永磁极弧比对齿槽转矩的影响。其次,采用混合永磁转子结构降低齿槽转矩。通过分析得到了混合永磁体之间的尺寸和极弧比的约束条件,确定了与最小齿槽转矩相关的两种永磁体,有限元仿真验证了分析结果。最后,比较了使用和不使用混合永磁体的电机性能。比较结果显示,采用本文提出的混合永磁体的转子结构,齿槽转矩显著降低。

关键词: 轴向磁通永磁同步电机; 转子结构; 齿槽转矩; 混合永磁; 极弧比